Impact Damage Sensing in Glass Fiber Reinforced Composites Based on Carbon Nanotubes by Electrical Resistance Measurements

Marco Monti, Maurizio Natali, Roberto Petrucci, José M. Kenny, Luigi Torre

University of Perugia, Civil and Environmental Engineering Department, Strada di Pentima 4, Terni 05100, Italy

Received 22 July 2010; accepted 20 February 2011
DOI 10.1002/app.34412
Published online 29 June 2011 in Wiley Online Library (wileyonlinelibrary.com).

ABSTRACT: In this article, we report an interesting employment of multi-walled carbon nanotubes as a filler in the epoxy matrix of a glass fiber reinforced composite (FRP). The intrinsic electrical conductivity of carbon nanotubes made the development of a nanocomposite with enhanced electrical properties possible. The manufactured nanocomposite was subsequently employed in the production of a glass FRP. Due to the high aspect ratio of carbon nanotubes, very small amounts of these particles were sufficient to modify the electrical properties of the obtained glass fiber composites. Basically, a three-phases material was developed, in which two phases were electrically insulating—epoxy matrix and glass fiber—and one phase highly conductive, the carbon nanotubes. The main goal of this study was to investigate the possibility of developing a glass fiber reinforced nanocomposite (GFRN), which is able to provide measurable electrical signals when subjected to a low-velocity impact on its surface. Following this goal, the drop in the mechanical performance of the composite was evaluated before and after the impact. At the same time, the variation in its electrical resistance was measured. The results have shown that it is possible to associate the increase in electrical resistance of the composite with the formation of damages caused by impact. © 2011 Wiley Periodicals, Inc. J Appl Polym Sci 122: 2829–2836, 2011

Key words: nanocomposites; thermosets; carbon nanotube

INTRODUCTION

The increasing use of fiber reinforced composites (FRP) in the aerospace, naval, and automotive industries, due to their high specific strength and stiffness, is directly connected to an increase in the need to monitor the status of the structure in which the FRP is utilized. In fact, the mechanical performance of composite materials may be severely reduced in the presence of damage produced by impact to the surface. This damage can either be fully invisible or barely visible (BVID) to the naked eye. These damages constitute an important limitation in the use of any structure,[1] as a wide variety of damage modes, such as matrix cracking, delaminations, debonding and fiber failure in composite structures are easily induced by an impact.

The monitoring of the status of a structural material is commonly carried out between two subsequent uses. However, the possibility in performing real-time monitoring is very attractive for the industrial market: it reduces inspection times, which obviously reduces the waste of money and even more importantly, guarantees safer employment of the structure. For this reason, in the past years, many researchers have been spending time and efforts on structural health monitoring (SHM) systems, developing new nondestructive inspection techniques which are exploitable directly in real-time or trying to convert traditional existing technologies into new real-time SHM systems.

As examples, some of the nondestructive inspection techniques commonly employed are acoustic emission (AE) based sensors and ultrasonic waves based technology.[2,3] Other techniques which are worth mentioning are the so-called comparative vacuum monitoring (CVM) techniques,[4] which include the use of fine tube-based sensors in which the vacuum is exploited for monitoring crack propagation and damages in structures and fiber Bragg diffraction grating sensors,[5] consisting of fiber-optic cables embedded in the structure, where any local strain causes a slight change in the sensor's light transmission wavelength.

The use of techniques that exploit the electrical properties of the composite have been widely recognized as a noninvasive way to monitor damage in carbon fiber reinforced plastic, due to the good electrical conductivity of the carbon fibers themselves.[6–18] In fact, they can act as electric conductors included in an insulating material, such as a thermosetting

Correspondence to: L. Torre (torrel@unipg.it).

matrix. When applying a mechanical load to the composite, the electrical resistance variation in the composite can be associated to a change in the conductive path of the carbon fibers. This piezoresistive behavior of carbon fiber composites have been demonstrated since the late eighties.[6] On the other hand, carbon fiber composites have revealed to be very sensitive to the damage produced by impact: different failure modes, which consist of fiber breaks, intra laminar cracks, as well as inter laminar delamination and debonding, can be detected by electrical measurements with an efficient positioning of the electrical contacts.[14–17]

In the last decade, researchers have demonstrated that it is possible to successfully employ electrically conductive nanoparticles, dispersed in plastics, to obtain a polymeric nanocomposite with enhanced electrical conductivity.[19–27] If such nanocomposites are used as a matrix in a nonconducting fiber composite, such as glass or aramid, it is possible to obtain a FRP with improved electrical properties which can be employed in advanced applications.

Kupke et al.[20,21] have shown how carbon black (CB) can improve the electrical conductivity of a glass fiber reinforced epoxy resin and how this novel nanocomposite shows piezoresistive behavior. On the other hand, carbon nanoparticles with high aspect ratios, namely carbon nanotubes and nanofibers, can overcome the electrical conductive threshold at very low concentrations if adequately mixed.[22–27]

Glass fiber reinforced nanocomposites (GFRN) based on carbon nanotubes have been widely studied for their potential functionality as sensors of strain and damage in themselves, demonstrating that both strain accumulation and damage formation can be detected by modifications in electrical resistance.[28–35]

In this study, the enhanced conductive properties of an epoxy-CNT nanocomposite were exploited to produce a glass FRP, in which the drop in mechanical performance due to impact, is strictly related to an increase in electrical resistance.

EXPERIMENTAL

A low-viscosity epoxy resin, supplied by Hexion under the commercial name of RIM 235, was employed as a matrix. Multi-walled carbon nanotubes (MWNTs) were employed as a nanofiller. They were supplied by CNT Co. (Korea) under the commercial name of C_{Tube}-100. As claimed by the technical data sheet, they have an average diameter in the range of 10–40 nm, a length between 1 and 25 microns and a purity of 93%.

The dispersion procedure consisted of several steps. At first, carbon nanotubes were added to the liquid epoxy monomer. A high-speed mechanical stirring technique (for 30 min) was exploited to disaggregate the nanotube agglomerations. Afterwards, an ultrasound bath (for 1 h) was used to improve the homogeneity of the dispersion and to degas the mixtures.

The dispersion degree was evaluated by TEM analysis, performed with a TEM Philips EM 208.

At the beginning of this study, the electrical behavior of the epoxy-based nanocomposite as a function of the nanoparticle content, was analyzed. To achieve this, mixtures with various contents of CNTs were produced, from 0.1 to 0.5 wt %. 0.5 wt % represented the maximum limit because at this concentration, the viscosity of the mixture increased too much and therefore processing was seriously compromised. A Keithley electrometer 6517B, with a resistivity test fixture 8009, was employed for this characterization.

Glass fibers were chosen for the production of the composite laminates. In fact, thanks to their electrically insulating properties, it is possible to isolate the contribution to the electrical conductivity given by the matrix. E-Glass fibers were employed to produce a balanced symmetric laminate, constituted by woven roving fabrics and chopped strand mats as a reinforcement. eight plies were used in the stacking sequence, six woven rovings and two mats arranged in the following mode: $(\text{Mat}, 3\ \text{Rowings})_S$. Vacuum infusion was used for processing.

Once the composites were cured, they were cut and utilized for mechanical characterization. Two different sets of specimens were considered. The first one was directly tested for its tensile properties. The latter was first impacted and then characterized by tensile tests, to evaluate the drop in mechanical performance caused by the impact in terms of elastic modulus, residual tensile strength and failure strain. The electrical resistance of the second set of specimens, those which were impacted, was measured before and after the impact, to evaluate the change caused by the impact itself.

Regarding the electrical characterization, the way in which the current is forced to flow in the specimen is an important factor: it obviously depends on the electrical contact configuration. Many studies have been conducted on testing different configurations, to evaluate which one was the most sensitive to the presence of damage.[31–34] In this work, the chosen solution was to perform a DC two-probe resistance measurement, using metal vices holding the specimen in the impact equipment directly as electrodes. To enhance electrical contact and to ensure that no change in the contact surface at the electrodes occurs during the impact, a silver paint was applied to the contact surface between the vice and the specimen. In this way, due the small thickness of the laminate (2 mm), a simple system to get a

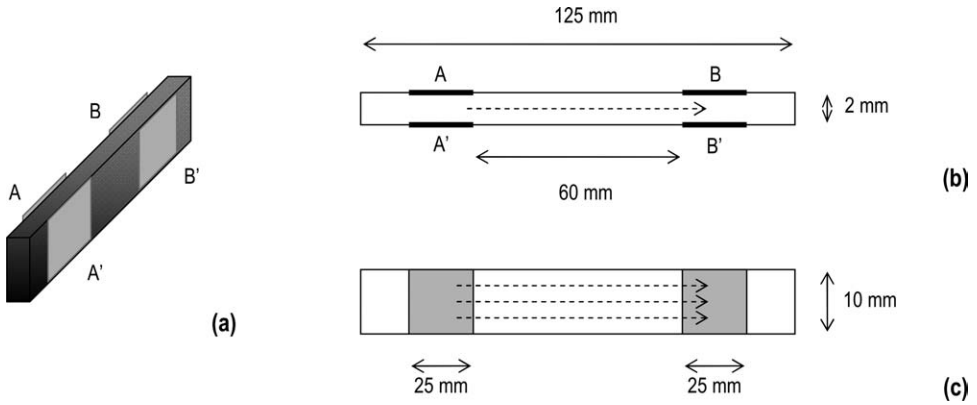

Figure 1 Electrical contact configuration. (a) global sketch; (b) through-thickness view; and (c) laminate surface view. Note that points A–A′ and B–B′ have the same potential (due to the metal sample holder). Dotted arrows indicate the current flow.

through-thickness measurement of the electrical current was realized. In Figure 1, the electrical contact configuration is summarized.

To make the impact tests, a self-made pendulum impactor was realized. A sphere with a diameter of 40 mm was employed as an impactor. It was left free to drop down from an angle of 90° and the energy absorbed by each specimen was calculated recording the angle reached by the impactor after the impact on its way back. The value of the impact energy was estimated as 11.7 J, and the impact velocity as 3.6 m/s. The impact energy was set to avoid the complete failure of the specimen, but enough to produce damage and was the same for all the tests. Ten specimens for each set were tested, to make an appropriate evaluation of the standard deviation of the results. In Figure 2, a schematic layout of the equipment and the test procedure are reported.

A dynamometer Lloyd Instruments, model LR30K, was utilized to perform mechanical tests, using extensometers to acquire the strain. The dimensions of the samples were 125 × 10 mm (the thickness of the laminate was 2.0 mm). The crosshead speed was set at 2 mm/min.

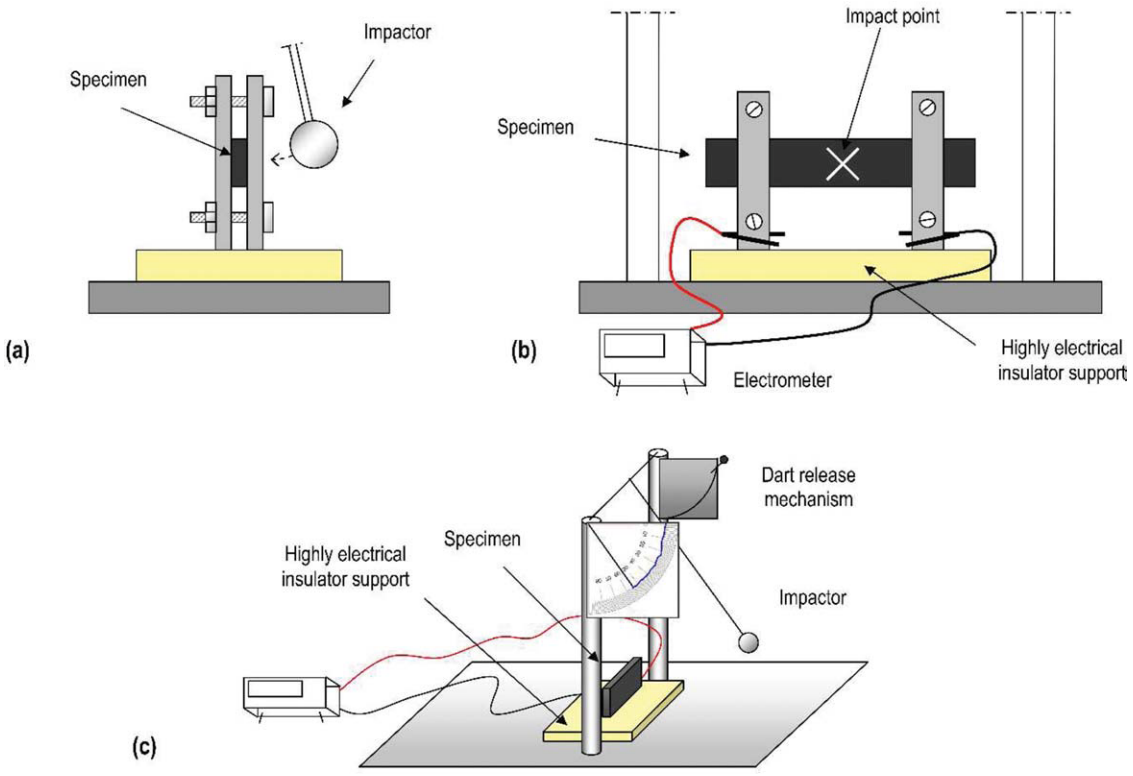

Figure 2 Schematic layout of the impact test: (a) side view; (b) frontal view; and (c) overview of the test layout [Color figure can be viewed in the online issue, which is available at wileyonlinelibrary.com.].

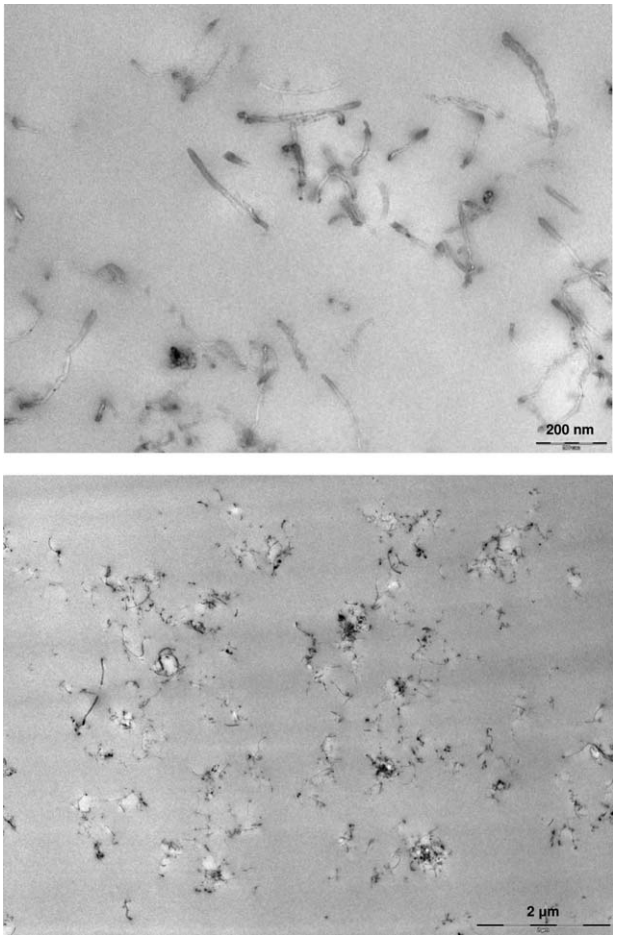

Figure 3 TEM micrograph of the 0.25%-CNT nanocomposite at two different magnifications.

To verify the consequences of the impact and to correlate the increased electrical resistance with the actual presence of damage, a morphological study on the through-thickness surface was carried out. A field emission scanning electron microscope (FESEM) ZEISS, model Supra 25, was utilized for these purposes.

RESULTS AND DISCUSSION

When working with nanocomposites, it is known that the maximum exploitation of the advantages of the nanoparticles are generally reached when uniform distribution and a good dispersion level are obtained. Figure 3 shows TEM images of the produced nanocomposites, with 0.25 wt % MWNTs at two different magnifications: beside areas in which it is possible to find fully de-bundled single nanotubes there are still zones where small agglomerations are present and zones where nanotubes are barely present. However, as will be shown, the dispersion level reached easily allowed us to cross the electrical percolation threshold at a very low nanotube content.

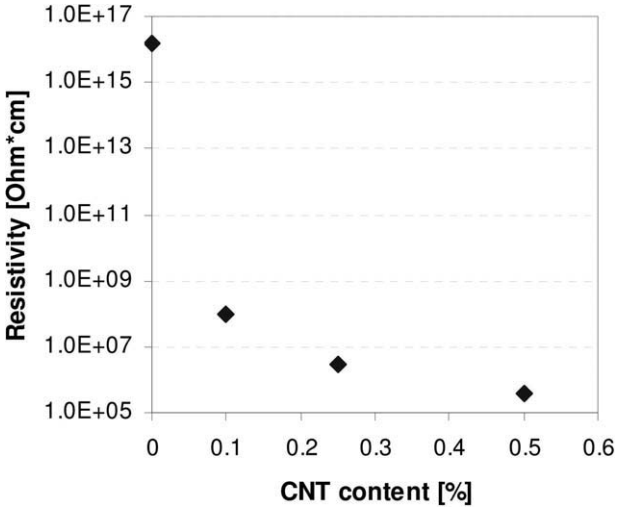

Figure 4 Electrical resistivity of the nanocomposites as a function of CNT content.

The outcome of the electrical characterization of the nanocomposites in Figure 4 shows electrical resistivity as a function of the CNT content. It is possible to observe a sharp decrease even at a CNT content of 0.1%, where the resistivity passes from 10^{16} to 10^{8} Ohm $\times$ cm, confirming the relevant role of carbon nanotubes in improving the electrical properties of polymers.

As a consequence thereof and taking into account the fact that the liquid mixture with a 0.5% content is completely unworkable due to its extremely high viscosity, the concentration of 0.25% CNT was chosen for the production of a nanocomposite-based FRP. The produced laminate presented a glass fiber volume fraction of about 45%, calculated with a calcination technique.

It has already been mentioned that an evaluation of the impact energy absorbed by the specimens was performed to correlate this amount of energy to the actual creation of damage inside the composite. Table I shows that about 54% of the energy associated to the impact was absorbed by the specimen.

As expected, the mechanical characterization of pristine and impacted specimens have shown that while damaging the composite, the impact strongly affected its performance. An example of the change in the mechanical trend due to impact in Figure 5 reports the stress–strain curve of a specimen before the impact and of an impacted specimen.

A more detailed characterization of the mechanical performance of the composite is reported in Figure 6,

TABLE I
Impact Energy Data

Impact energy [J]	11.7
Energy absorbed [J]	6.4 ± 1.2
Part of the impact energy absorbed [%]	54.3 ± 0.7

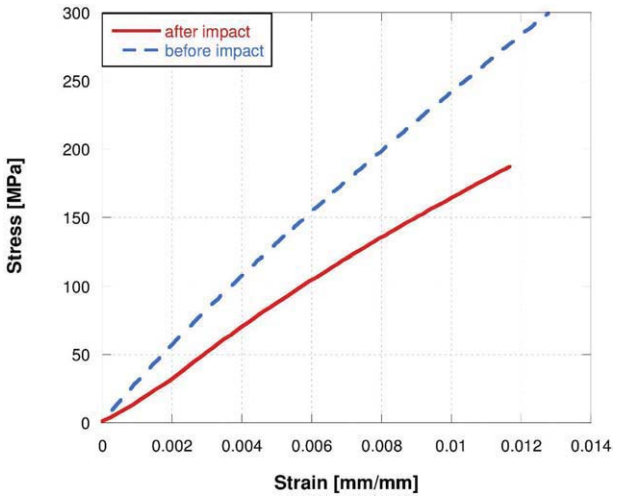

Figure 5 Representative stress–strain curve of pristine and impacted specimens [Color figure can be viewed in the online issue, which is available at wileyonlinelibrary.com.].

where Young modulus, tensile strength, and strain to failure are plotted. All these properties tend to drop significantly, in particular the highest decrease was in the tensile strength, which passed from 300 MPa to a little over 150 MPa. Both Young modulus and elongation at break show a drop of about 30% with respect to the initial value after the impact.

To verify this consideration and investigate the morphology of the damage produced by the impact,

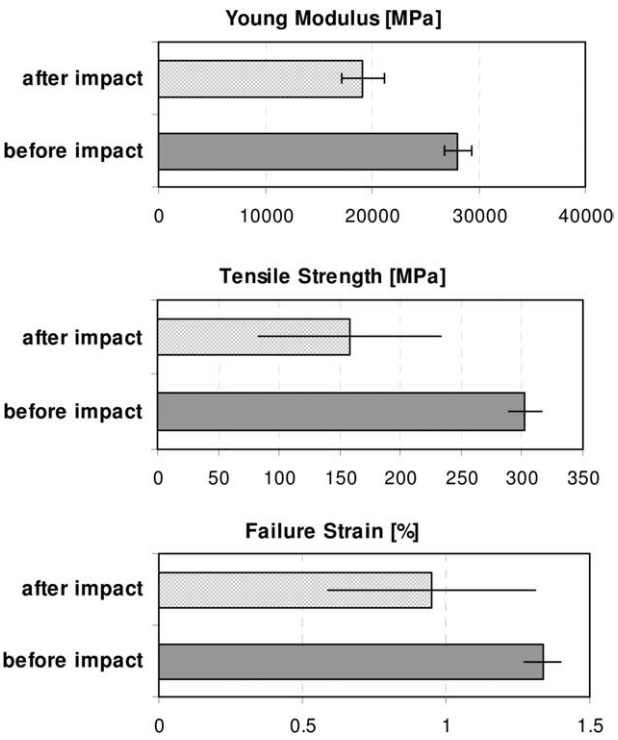

Figure 6 Tensile properties of pristine and impacted specimens.

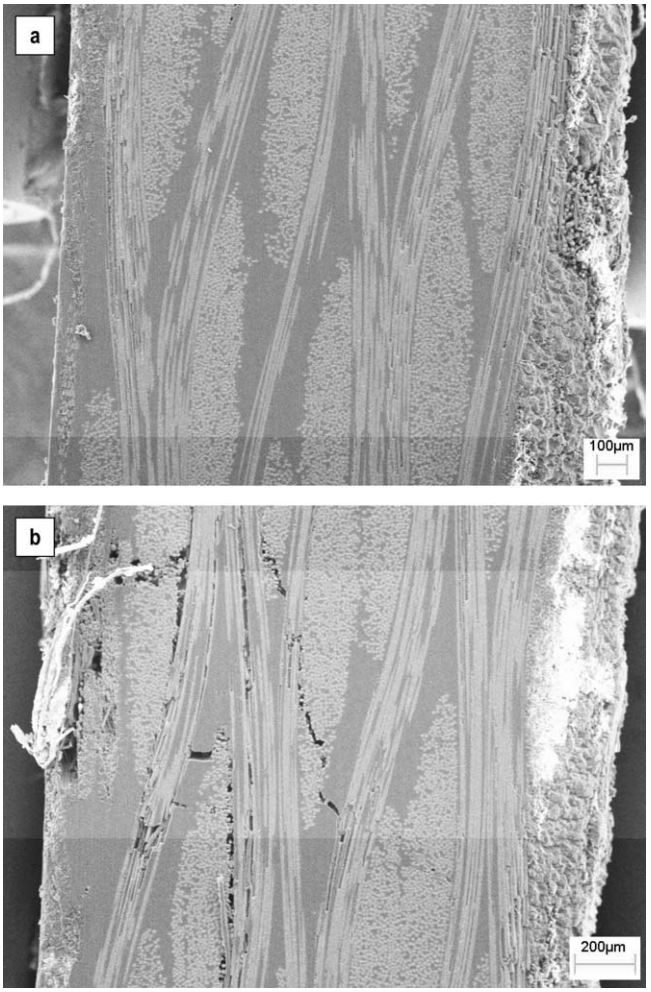

Figure 7 FESEM images of the through-thickness surface of the composite (a) preimpact, (b) postimpact.

FESEM images were taken on the through-thickness surface of the samples after the impact. Figure 7 shows the transversal surface of a specimen, before (a) and after the impact (b). Figure 7(a) confirms that the composite produced was void and micro-crack free. Note that the right surface is quite rough as a consequence of the presence of a vacuum bag during processing.

The considerable drop in mechanical properties due to the impact is obviously related to the actual overcoming of the preinitial fracture region,[36] in which the impact energy is fully absorbed, as strain energy by the elastic deformation of the composite. More precisely, in this preinitial fracture region, the impact energy is stored mainly by the elastic deformation of the 0° fibers. In fact, in this phase, the contribution in stored energy of the matrix and the 90° fibers is negligible. The failure of the studied composite consists of several fracture modes, as it is possible to observe in Figure 7(b). Fiber pull out is visible at the bottom of the specimen, i.e., in the surface opposite to the impact and in exact correspondence

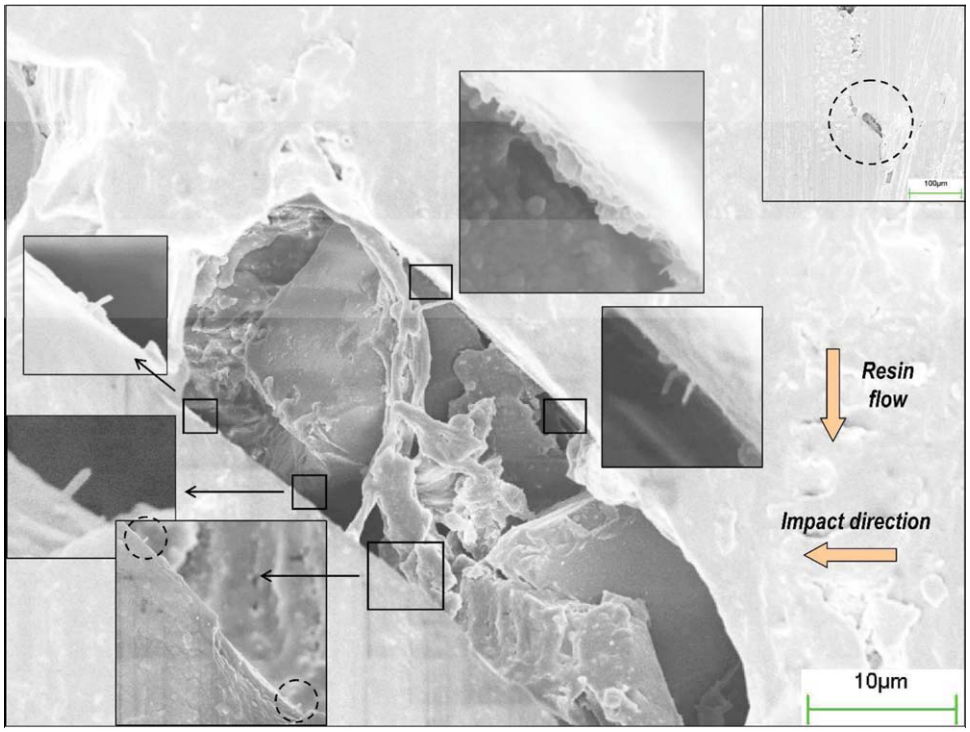

Figure 8 FESEM image of a representative micro-crack morphology in the composite [Color figure can be viewed in the online issue, which is available at wileyonlinelibrary.com.].

to the impacted area. Furthermore, transversal micro-cracks which involve more than one ply, as well as intralamina cracks are clearly present in the cross-sectional area of the specimen, starting from behind the impact area and extending in both directions. At the same time, the cross-sectional area also exhibits delamination effects.

A higher magnification inspection of the damaged through-thickness surface can explain the role of carbon nanotubes in the composite. Figure 8 shows a micro-crack caused by the impact with various enlargements. It is clear that the failure mechanism of the composite, regarding the interphase CNT-epoxy, occurred due to the pullout of the nanotubes from the matrix. The preferential orientation of the nanotubes in the direction perpendicular to the impact direction was due to the processing conditions. It has already been pointed out that the composite laminate was produced using a vacuum infusion technique and the tendency of the nanotubes to be oriented towards the flow direction is to be expected due to shear flow. From this figure, it is clear that the carbon nanotubes acted as a bridge in the resin, creating a conductive pathway for the electrical current flow. The role of conductive mediums exerted by carbon nanotubes in a glass fiber composite and by carbon fibers in a carbon fiber composite is schematically reported in Figure 9. On comparing them, it is possible to state that, although the contribution given by the nanotubes is less effective in terms of the final electrical conductivity of the composite, the produced effect is more homogeneous, that is, the conductive network is less bound to the direction in which the current is forced to pass through the composite. This occurs as a result of the random distribution of nanotubes in the matrix, although a preferential orientation is produced during the vacuum infusion process.

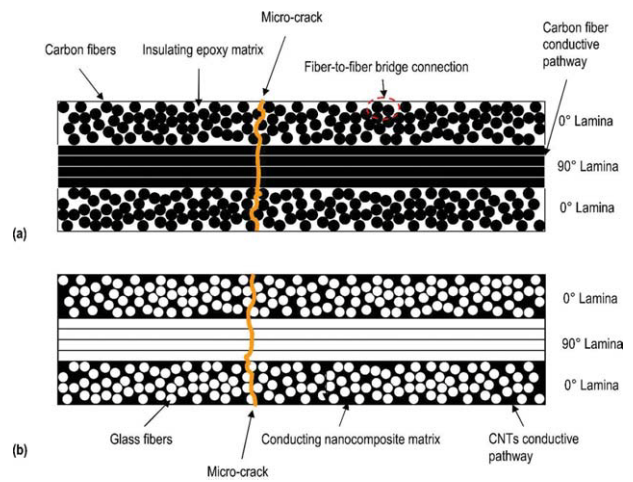

Figure 9 Schematic representation of the conductive mechanism in a carbon fiber composite (a) and in a glass fiber composite based on a CNT-doped matrix (b) [Color figure can be viewed in the online issue, which is available at wileyonlinelibrary.com.].

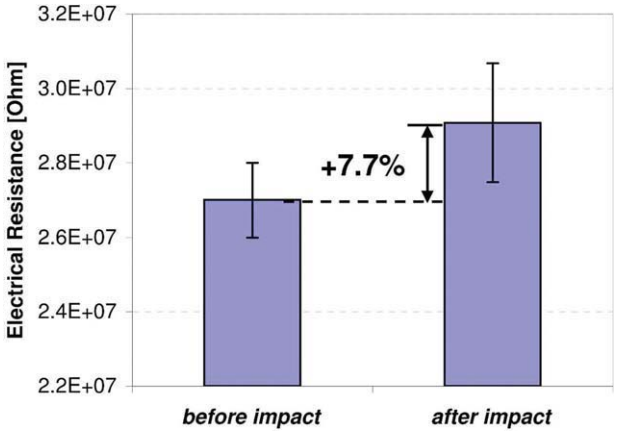

Figure 10 Electrical resistance variation in the sample preimpact (a) and postimpact (b). Both the reported values are averaged between longitudinal and transversal directions [Color figure can be viewed in the online issue, which is available at wileyonlinelibrary.com.].

These considerations of the conductive pathway are needed to explain the results of the electrical characterization. First, a difference in electrical resistance of the virgin samples (R_0) was found between the direction parallel and perpendicular to the resin flow. The electrical resistance of longitudinal cut specimens was evaluated as 2.1 ($\pm$0.6) $\times$ 10^7 Ohm, whereas the other was 3.3 ($\pm$0.7) $\times$ 10^7 Ohm was measured. Although both quite high values, they are still well measurable resistance using the adequate equipment. Regardless of the longitudinal or transversal cut of the specimen, the measurement of the electrical resistance after the impact has demonstrated that an increase of about 7.7 ($\pm$2.1) % is observed, as a consequence of the impact itself (Fig. 10), calculated as $\Delta R/R_0$.

A step increase in electrical resistance as a consequence of the damage created by impact in carbon fiber-based composites without the aid of a conducting matrix was also found in other literature.[17] In this system, where the conductive pathway only consists of carbon fibers, an increase in electrical resistance is produced by fiber breaks and fiber-to-fiber bridging connection openings. The analogous results obtained in our study suggests that, even in this case, a step increase in electrical resistance is due to the deterioration of the conductive network, which is formed here by the carbon nanotubes embedded in the matrix and not by the carbon fabric filaments.

This means that an adequate measurement of electrical resistance allows one to detect damages that have not caused the catastrophic failure of the composite but have affected its mechanical performance, since its tensile and failure strain were reduced by 50 and 30%, respectively. Therefore, the use of a CNT-doped matrix permits the production of composites whose status can be adequately monitored using simple electrical measurements.

CONCLUSIONS

A MWNT-based epoxy nanocomposite with enhanced electrical conductivity with respect to the neat resin, was successfully developed. A content of 0.25 wt % was evaluated as the best compromise between the improved electrical properties and the increase in viscosity. Consequently, it was possible to produce a glass FRP, based on this nanocomposite, using a liquid molding technique such as vacuum infusion.

The FRP produced was subjected to an impact able to reduce its mechanical performance. Despite the reduction in its mechanical properties, the composite still maintained more than 50% of its initial properties, which means that the damage produced did not imply the catastrophic failure of the composite. Nonetheless, this damage is associated to a significant increase in electrical resistance. Therefore, the measurement of the electrical resistance of CNT-doped glass FRPs can be considered a good method for monitoring the presence of impact damage.

The authors thank Mr. Sandro Andrielli and Mr. Giorgio Monti for their useful contribution in designing and producing the impact device. Authors also thank Mr. Marco Rallini for the SEM analysis.

References

1. Polimeno, U.; Meo M. Compos Struct 2009, 91, 398.
2. Fu, T.; Liu, Y.; Li, Q.; Leng, J. Opt Laser Eng 2009, 47, 1056.
3. Finlayson, R. D.; Friesel, M.; Carlos, M.; Cole, P.; Lenain, J. C. Insight 2001, 43, 3.
4. Roach, D. Smart Struct Syst 2009, 5, 317.
5. Lam, P.; Lau, K.; Ling, H.; Su, Z.; Tam, H. Opt Laser Eng 2009, 47, 1049.
6. Schulte, K.; Baron, Ch. Compos Sci Technol 1989, 36, 63.
7. Wang, S.; Chung, D. D. L. Polym Compos 2000, 21, 13.
8. Abry, J. C.; Bochard, S.; Chateauminois, A.; Salvia, M.; Giraud, G. Compos Sci Technol 1999, 59, 925.
9. Todoroki, A. Key Eng Mater 2004, 270, 1812.
10. Todoroki, A.; Yoshida, J. JSME Int J A 2004, 47, 357.
11. Ogi, K.; Takao, Y. Compos Sci Technol 2005, 65, 231.
12. Todoroki, A.; Omagari, K.; Shimamura, Y.; Kobayashi, H. Compos Sci Technol 2006, 66, 1539.
13. Ceysson, O.; Salvia, M.; Vincent, L. Script Mater 1996, 34, 1273.
14. Wang, D.; Chung, D. D. L. Smart Mater Struct 2006, 15, 1332.
15. Angelidis, N.; Irving, P. E. Compos Sci Technol 2007, 67, 594.
16. Angelidis, N.; Khemiri, N.; Irving, P. E. Smart Mater Struct 2005, 14, 147.
17. Wang, D.; Chung, D. D. L.; Chung, J. H. Compos Part A 2005, 36, 1707.
18. Meehan, D. G.; Wang, S.; Chung, D. D. L. J Intel Mater Syst Struct 2010, 21, 83.
19. Flandin, L.; Cavaille, J.-Y.; Brechet, Y.; Dendievel, R. J Mater Sci 1999, 34, 1753.
20. Kupke, M.; Wentzel, H.-P.; Schulte, K. Mater Res Innovat 1998, 2, 164.

21. Kupke, M.; Schulte, K.; Schüler, R. Compos Sci Technol 2001, 61, 837.
22. Liang, G. D.; Tjong, S. C. Mater Chem Phys 2006, 100, 132.
23. Hammel, E.; Tang, X.; Trampert, M.; Schmitt, T.; Mauthner, K.; Eder, A.; Peotschke, P. Carbon 2004, 42, 1153.
24. Sandler, J.; Shaffler, M. S..P.; Prasse, T.; Bauhofer, W.; Schulte, K.; Windle A. H. Polymer 1999, 40, 5967.
25. Bryning, M. B.; Islam, M. F.; Kikkawa, J. M.; Yodh, A. G. Adv Mater 2005, 17, 1186.
26. Vera-Aguillo, J.; Gloria-Pereira, A.; Varela-Rizo, H.; Gonzalez, J. L.; Martin-Guillon, I. Compos Sci Technol 2009, 69, 1521.
27. Monti, M.; Terenzi, A.; Natali, M.; Gaztelumendi, I.; Markaide, N.; Kenny, J. M.; Torre, L. J Appl Polym Sci 2010, 117, 1658.
28. Thostenson, E. T.; Chou, T. W. Adv Mater 2006, 18, 2837.
29. Gojny, F. H.; Wichmann, M. H. G.; Fiedler, B.; Bauhofer, W.; Schulte, K. Compos Part A 2005, 36, 1525.
30. Böger, L.; Wichmann, M. H. G.; Meyer, L. O.; Schulte, K. Compos Sci Technol 2008, 68, 1886.
31. Wichmann, M. H. G.; Sumfleth, J.; Gojny, F. H.; Quaresimin, M.; Fiedler, B.; Schulte, K. Eng Fract Mech 2006, 73, 2346.
32. Thostenson, E. T.; Chou, T.W. Nanotechnology 2008, 19, 215713.
33. Gao, L. M.; Thostenson, E. T.; Zhang, Z. G.; Chou, T. W. Adv Funct Mater 2009, 19, 123.
34. Chou, T. W.; Gao, L. M.; Thostenson, E. T.; Zhang, Z. G.; Byun, J. Compos Sci Technol 2010, 70, 1.
35. Zhang, R.; Baxendale, M.; Peijs, T. Phys Rev B 2007, 76, 195433.
36. Mallick, P. K. Fiber Reinforced Composites, 3rd ed.; CRC Press: New York, 2007.